

Intercalated Cu⁺ ion dynamics in the two-dimensional layered compound Cu_{0.33}TiSe₂

Shunsuke Kitou^{1,*}, Takumi Hasegawa,² Akitoshi Nakano,³ Naoyuki Katayama,¹ Satoshi Tsutsui,⁴ and Hiroshi Sawa^{1,†}

¹Department of Applied Physics, Nagoya University, Nagoya 464–8603, Japan

²Graduate School of Integrated Arts and Sciences, Hiroshima University, Higashi-Hiroshima, Hiroshima 739–8521, Japan

³Department of Physics, Nagoya University, Nagoya 464–8602, Japan

⁴Japan Synchrotron Radiation Research Institute (JASRI), SPring-8, Hyogo 679–5198, Japan



(Received 8 November 2019; revised manuscript received 8 March 2020; accepted 10 March 2020;
published 31 March 2020)

Cu⁺ ion behavior is one of the heavily discussed topics in physical and material fields because of its unclear behavior and high potential in materials application. To provide a breakthrough in this field, comprehensive research that connects the real space and the reciprocal lattice (momentum) space is effective. Here, we investigated the Cu⁺ ion behavior in two-dimensional layered system Cu_{0.33}TiSe₂, which shows the Cu⁺ disorder-order phase transition at 200 K. Inelastic x-ray scattering revealed a large change of the Cu⁺ ion dynamics at the phase transition. It is expected that the complex interactions are involved in the behavior of Cu⁺ ions intercalated in the negatively charged TiSe₂ layers by charge transfer. However, Monte Carlo simulations using a simple combination of repulsive forces between Cu⁺ ions well reproduce the characteristic temperature dependence of the anisotropic diffuse scattering. These insights provide a unified understanding in controlling the intercalated system.

DOI: [10.1103/PhysRevB.101.094108](https://doi.org/10.1103/PhysRevB.101.094108)

I. INTRODUCTION

The disorder-order phase transition is a common phenomenon observed in various systems such as water [1], alloys [2], magnetic material [3], and dielectric material [4], where the control parameters are sometimes very complicated due to the cooperation and/or competition of various interactions. Recently, the two-dimensional (2D) layered compounds in which ions are inserted between layers have garnered significant attention not only for their fundamental physical properties [5–9] but also for their applications as ion conductive and thermoelectric materials [10–13], where the disorder-order phase transitions of interlayer ions are often observed [9–11]. In these systems, understanding and controlling the behavior of the interlayer ions is required to improve material properties.

The transition-metal dichalcogenide series 1T-TiSe₂ has been of particular interest to researchers for decades because it displays interesting electronic behavior such as excitonic phase [14–20], superconductivity [21], charge-density wave (CDW) [9,22], and Cu⁺ ordering [9] through Cu⁺ intercalation that results in electron doping from Cu⁺ ions. In particular, Cu_{0.33}TiSe₂, which has a magic number 1/3 of the amount of Cu⁺ ion, shows the disorder-order phase transition caused by Cu ordering at $T_c = 200$ K [9] [Figs. 1(a) and 1(b)]. In addition, a honeycomb-lattice-type CDW is observed in TiSe₂ layers arising from the Cu_{1/3}-ordered phase.

Although the Cu ordering plays an important role in the CDW phase transition of the host framework, the state of

Cu⁺ ion in the high-temperature (HT) phase is not well understood [9]. In the low-temperature (LT) phase, Cu⁺ ions are completely ordered in plane in the $(\sqrt{3}a \times \sqrt{3}b)_{\gamma_2}$ arrangement [Fig. 1(b)]. On the other hand, in the HT phase, x-ray-diffraction (XRD) experiments reveal the characteristic diffuse scattering in the a^*b^* plane. When the crystal structural analysis was performed ignoring the diffuse scattering intensity in the HT phase, the partial site occupancy of ~33% Cu⁺ between the upper and lower TiSe₆ octahedra was confirmed [Fig. 1(a)]. Although these results suggest a dynamical motion of Cu⁺ ions near room temperature, the behavior of Cu⁺ ions remains mysterious, especially its dynamics and the origin of the characteristic diffuse scattering pattern.

In the exploration of postlithium systems, it is preferable to find safer, less expensive, and more sustainable alternatives such as Cu⁺ ion conductive materials for energy applications [23,24]. Thus, it is important to understand the Cu⁺ ion behavior not only for elucidating the electronic state of Cu_{0.33}TiSe₂ system but also for the material design of intercalated layered compounds. In this paper, the phase-transition mechanism and the Cu⁺ ion behavior in Cu_{0.33}TiSe₂ are investigated using synchrotron XRD, inelastic x-ray scattering (IXS), first-principles calculations, and Monte Carlo (MC) simulations.

II. METHOD

A. Experiments

Cu_{0.33}TiSe₂ single crystals were synthesized according to a method reported previously [25]. The XRD experiments were conducted using a BL02B1 beamline at the synchrotron facility SPring-8 in Japan [26] with a wavelength of

*kitou.shunsuke@h mbox.nagoya-u.ac.jp

†hiroshi.sawa@cc.nagoya-u.ac.jp

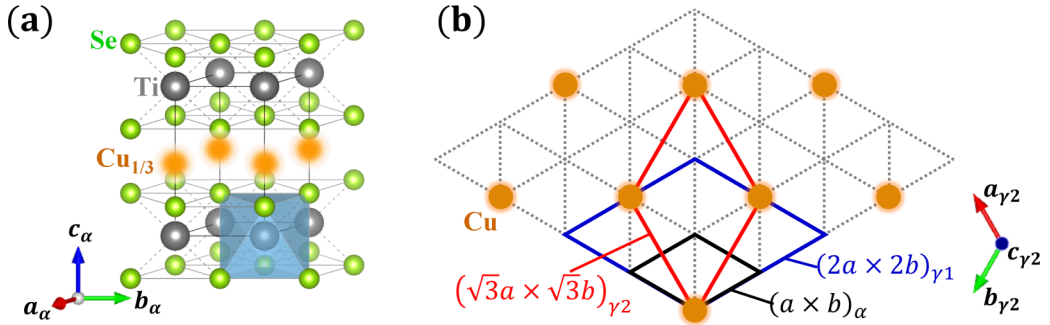


FIG. 1. (a) Crystal structure of Cu_{0.33}TiSe₂ in the HT phase. (b) Cu_{1/3}-ordering pattern in the LT phase. Black rhombus indicates the unit-cell size of the HT phase. Blue and red rhombuses indicate the unit-cell size of the Cu_{1/4}-ordered phase (γ_1 phase of Cu_{1/4}TiSe₂) and Cu_{1/3}-ordered phase (γ_2 phase of Cu_{1/3}TiSe₂), respectively [9].

0.355 10 Å. The dimensions of the Cu_{0.33}TiSe₂ single crystal used for the XRD experiment were 200 × 120 × 20 μm³. A He-gas-blowing device was employed to cool the sample to 30 K. A 2D CdTe PILATUS detector was utilized with the diffractometer. The IXS experiments were conducted using a BL35XU beamline at SPring-8 [27]. A Si (11, 11, 11) backscattering setup with an energy resolution of 1.5 meV and a wavelength of 0.570 11 Å (21.747 keV) was chosen for our study. A Cu_{0.33}TiSe₂ single crystal (1800 × 1400 × 15 μm³) was mounted on a closed-cycle cryostat installed on an IXS spectrometer. The Q resolution was (0.05, 0.05, 0.03) in reciprocal lattice units.

B. First-principles calculations

The first-principles calculations of the phonon modes in Cu_{0.33}TiSe₂ in the LT phase were performed using the ABINIT package [28,29] with the local-density approximation (LDA) parametrized by Perdew and Wang [30] and the projector augmented-wave method [31,32]. The partial waves and projector functions were generated by ATOMPAW [33] with valence configurations of 3d⁹4s² for Cu, 3s²3p⁶4s²3d² for Ti, and 4s²4p⁴ for Se. The plane-wave cutoff energy was 490 eV, and the k -point mesh on the 12 × 12 × 2 Monkhorst-Pack grid [34] in the LT-phase Brillouin zone was used. The Fermi-Dirac distribution with $T = 27$ meV was applied, since Cu_{0.33}TiSe₂ is metallic according to the LDA result. The interatomic force constants were obtained via the density-functional perturbation theory (DFPT) [35,36] on the 6 × 6 × 2 grid. The IXS spectra were calculated according to Ref. [37].

C. MC simulations

The system size was a 60 × 60 × 1 cell for our MC simulations. The total energy can be expressed as $E = \sum_{(i,j)} U_{ij} w_i w_j$, where w_i , w_j (=1 or 0) are occupancies of the i th and j th sites, and U_{ij} is the pair-interaction strength between the i th and j th sites. In this study, we considered only the first, second, and third nearest-neighbor interactions as U_1 , U_2 , and U_3 , respectively, whose distances correspond to a , $\sqrt{3}a$, and $2a$, respectively [see Fig. 4(a)]. Temperature changes using the Metropolis method [38] were performed in the range of $0 \leq T \leq 1$ on cooling.

III. RESULT AND DISCUSSION

A. Cu⁺ ion dynamics

To obtain information about the Cu⁺ ion dynamics in Cu_{0.33}TiSe₂, IXS experiments and DFPT calculations were performed. Since the diffuse scattering appeared strongly along the pink lines in the first Brillouin zone in the HT phase [Fig. 2(a)], the IXS measurements were conducted on the $L-H-A$ path, indicated by the green arrow in Fig. 2(a). Figure 2(b) shows the color plot of the energy spectra obtained from the IXS measurements at 150 K (LT phase). Figure 2(c) presents the results of the DFPT calculations in the LT phase, corresponding to Fig. 2(b). The superlattice reflection intensity in the actual LT phase appears at the H point; therefore, the dispersion of the acoustic mode of TiSe₂, which exists at the H point in Fig. 2(c), cannot be clearly observed from the IXS measurements. In the other regions of the Brillouin zone, the results of the IXS experiments and DFPT calculations agree well.

Our DFPT calculations show that the vibrational mode corresponding to the honeycomb-lattice-type CDW in the TiSe₂ layers (Supplemental Material, Fig. S4 [39]) exists with a very weak intensity at ∼16 meV at the H point. This softening mode of the CDW transition in Cu_{0.33}TiSe₂ is completely different from softening of the transverse optical phonon mode observed in the excitonic phase transition in pristine 1T-TiSe₂ [40]. However, it was impossible to extract the spectrum corresponding to the softening mode of the honeycomb-lattice-type CDW from the IXS experiment due to the interference from the superlattice reflection intensity. On the other hand, the change in the vibrational mode of TiSe₂, which will be affected by Cu ordering, was confirmed to occur at T_c near the A point (Fig. S5 [39]).

The vibrational mode of Cu⁺ ions [E_g^{Cu} mode, inset of Fig. 2(d)] occurs at ∼12 meV (A point) in Fig. 2(c). Although the E_g^{Cu} mode cannot be clearly confirmed from the 2D color plot in Fig. 2(b), the one-dimensional (1D) IXS spectra at the A point [Fig. 2(d)] clearly show the peak corresponding to the E_g^{Cu} mode at ∼9 meV. The differences in the peak positions of the E_g^{Cu} mode between the IXS experiment and DFPT calculations are due to the smaller lattice constants of the optimized structure in the DFPT calculations (experiment: $a_{\gamma_2} = 6.1540$ Å, $c_{\gamma_2} = 12.1834$ Å at 150 K; calculations: $a_{\gamma_2} = 5.9797$ Å, $c_{\gamma_2} = 11.7979$ Å).

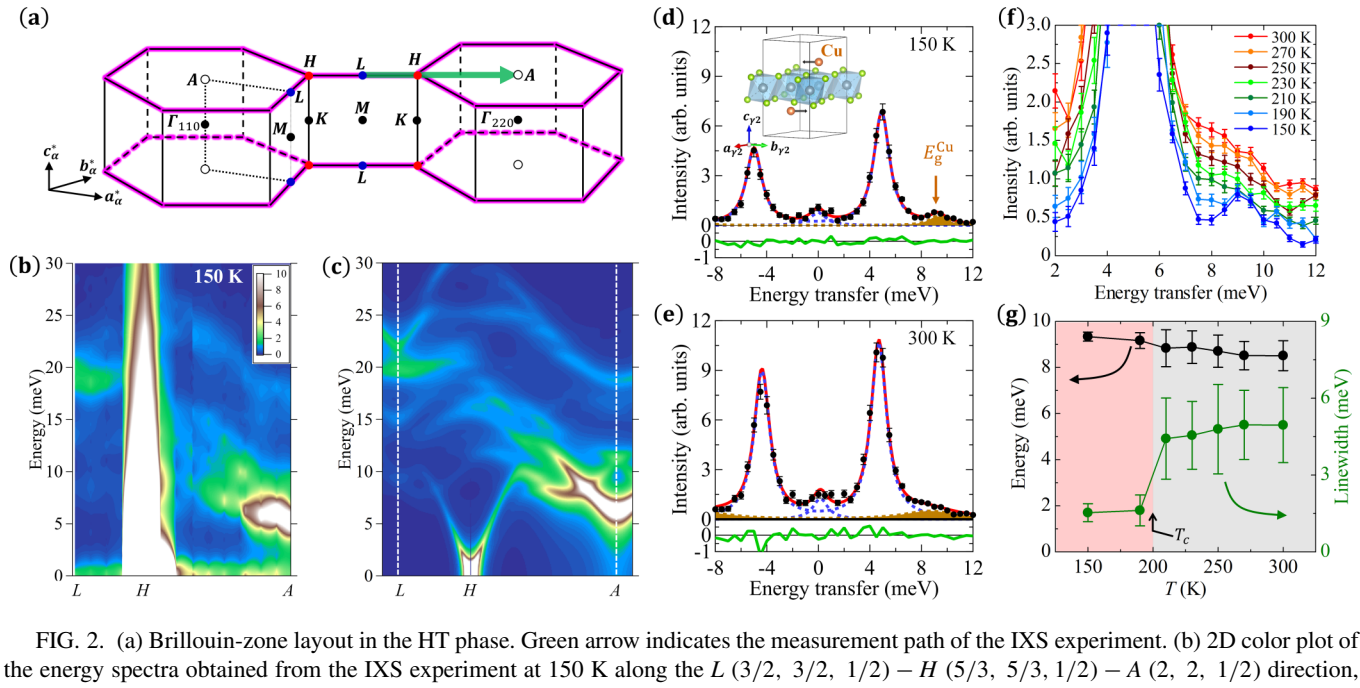


FIG. 2. (a) Brillouin-zone layout in the HT phase. Green arrow indicates the measurement path of the IXS experiment. (b) 2D color plot of the energy spectra obtained from the IXS experiment at 150 K along the $L(3/2, 3/2, 1/2) - H(5/3, 5/3, 1/2) - A(2, 2, 1/2)$ direction, whose \mathbf{k} points are defined in the HT phase. (c) 2D color plot of the energy spectra obtained from the DFPT calculation, which is displayed with an energy resolution of 1.5 meV. 1D IXS spectra of the $A(2, 2, 1/2)$ point at (d) 150 K and (e) 300 K. Red line shows the result of the fitting using three Lorentz functions, corresponding to an elastic peak at 0 meV, the vibrational mode of TiSe_2 in the \mathbf{ab} plane at ~ 5 meV, and the vibrational mode of Cu^+ ions at ~ 9 meV (E_g^{Cu} mode; brown). Green line shows the differences between the acquired and the calculated spectra. Inset of (d): schematic of the collective vibrations of the E_g^{Cu} mode at ~ 9 meV. (f) Temperature dependence of the IXS spectra at the A point in the range of 150–300 K. (g) Temperature dependence of the peak energy and linewidth of the E_g^{Cu} mode.

The peak broadening of the E_g^{Cu} mode is observable above 200 K [Figs. 2(e) and 2(f)]. Figure 2(g) shows the temperature dependence of the peak energy and linewidth of the E_g^{Cu} mode. Although there is no significant change in the peak energy at T_c , the linewidth of the peak in the Cu-disordered phase increases to approximately three times that in the Cu-ordered phase. The change of the E_g^{Cu} mode suggests that the diffuse scattering observed in the XRD experiment is mainly due to the Cu^+ ion dynamics. Assuming that Cu^+ ions cannot move, the linewidth of the E_g^{Cu} mode in the LT phase corresponds to the lifetime of the vibrational mode of Cu^+ ions at each site. On the other hand, the linewidth in the HT phase increases by the additional scattering due to the changes of the Cu^+ ion dynamics and/or the environment of Cu^+ ions. One possible reason for this behavior is that Cu^+ ions can move by hopping around Cu^+ sites in the HT phase. The temperature dependence of the E_g^{Cu} mode in $\text{Cu}_{0.33}\text{TiSe}_2$ is similar to that of the vibration mode of Cu^+ ions in CuCrSe_2 [10] and Ag^+ ions in AgCrSe_2 [11], which are observed by the inelastic neutron scattering. However, these behaviors of interlayer ions in real space are not obvious.

B. X-ray diffuse scattering

The change of the Cu^+ ion dynamics seems to be understood by the short-range Coulomb interaction among Cu^+ ions. If the Coulomb repulsion only exists in the nearest-neighbor sites in the total occupancy of $1/3$, a perfect $\sqrt{3} \times \sqrt{3}$ structure would be realized in the ground state, as easily predicted. In fact, in the XRD data of the LT phase [Fig. 3(c)],

superlattice peaks appear at the H points, which correspond to the $\text{Cu}_{1/3}$ ordering of $(\sqrt{3}\mathbf{a} \times \sqrt{3}\mathbf{b} \times 2\mathbf{c})_{\gamma_2}$, and there is almost no intensity except around the reciprocal lattice points. However, the characteristic diffuse scattering appears

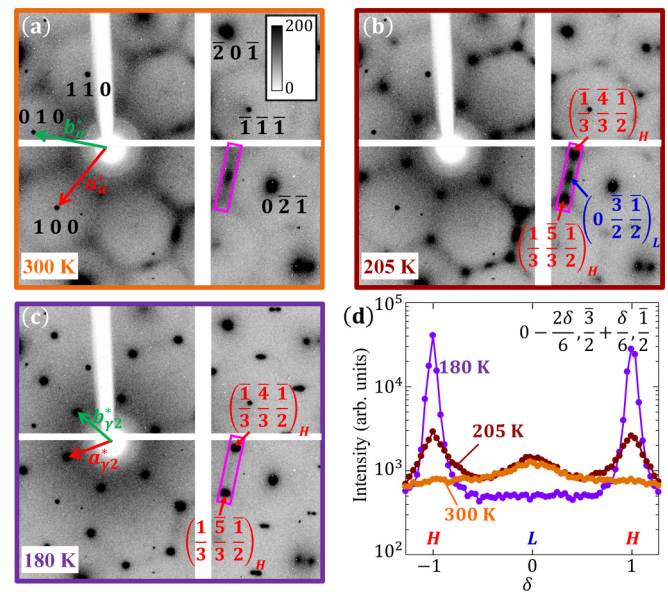


FIG. 3. (a)–(c) XRD data in plane at 300, 205, and 180 K, respectively. (d) Temperature dependence of diffuse scattering profiles corresponding to the intensity of the diffracted spots in pink rectangles in (a)–(c); the vertical axis follows a logarithmic.

at positions that are not H points in the HT phase [Figs. 3(a) and 3(b)]. Figure 3(d) shows the temperature dependence of the diffuse scattering profiles corresponding to the intensity in the pink rectangles in Figs. 3(a)–3(c). At 300 K [Fig. 3(a)], the honeycomb-lattice-type streaklike diffuse scattering exists with a relatively stronger intensity at the L points.

At 205 K [Fig. 3(b)], just above T_c , the intensity at the L points hardly changes, whereas the diffuse scattering intensity at the H points develops. The diffuse scattering at the H points corresponds to the $\text{Cu}_{1/3}$ ordering of $\text{Cu}_{0.33}\text{TiSe}_2$ in the LT phase (γ_2 phase). On the other hand, the diffuse scattering at the L points corresponds to the $2a \times 2b \times 2c$ structure, which may be related to the $\text{Cu}_{1/4}$ ordering of $(2a \times 2b \times 2c)_{\gamma_1}$ in $\text{Cu}_{0.24}\text{TiSe}_2$ in the LT phase (γ_1 phase) [9]. In the HT phase, two kinds of short-range interactions among Cu^+ ions develop near the phase transition. It is strange that the diffuse scattering intensity appears at the L points that do not match the $\text{Cu}_{1/3}$ -ordering pattern. In the case of 1/4-filling system, assuming only the nearest-neighbor Coulomb repulsion among Cu^+ ions, no Cu ordering is confirmed at the ground state as described later. These results are not consistent with the prediction considering only the individual interaction among Cu^+ ions. The diffuse scattering behavior may be due to the potential of the surrounding Ti and Se atoms and/or the shielding effect of conduction electrons, because the Cu^+ ions exist between TiSe_2 layers forming a frustrated triangular lattice.

C. Cu^+ ion behavior investigated by MC simulations

To understand the characteristic diffuse scattering behavior caused by Cu^+ ions, MC simulations using the Metropolis method [38] were performed. Since only one Cu layer was considered in the MC simulations, the H and L points in the actual system, where a double periodic structure is formed in the stacking direction, correspond to the K and M points, respectively, in the Brillouin-zone layout [Fig. 2(a)]. As mentioned above, when considering only the nearest-neighbor interaction U_1 ($U_1 = 1$ was set as the energy standard) as the total occupancy $\bar{w} = 1/3$ [Fig. 4(a)], the complete $\sqrt{3} \times \sqrt{3}$ (K -type) structure is certainly realized in the ground state [Fig. 4(d)] and there is no characteristic intensity at the M point above $T_c = 0.74$ [Fig. 4(c)].

Next, we considered the second and third nearest-neighbor interactions as U_2 and U_3 , respectively [Fig. 4(a)]. By increasing $U_2 > 0.2$, the 2×2 , 1×2 , 2×3 (M -type) structures or their combinations (Fig. S7 [39]) are realized in the ground state. All of these structures display superlattice peaks mainly at the M point. Figure 5(a) shows the $U_3/U_1 - U_2/U_1$ ground-state phase diagram, where the color scale indicates the difference between the intensities at the K and M points [$\text{Int.}(K) - \text{Int.}(M)$]. For color mapping, the intensities at $T = 0$ cooled from a random arrangement at $T = 1$ were used. Consequently, the phase boundaries between the K - and M -type structures exist along $\frac{U_3}{U_1} = \frac{5}{6} \frac{U_2}{U_1} - \frac{1}{6}$ and $(\frac{U_2}{U_1} \leqslant 0.2) \frac{U_3}{U_1} = \frac{5}{4} \frac{U_2}{U_1} - \frac{1}{4} (\frac{U_2}{U_1} \geqslant 0.2)$ dotted lines in Fig. 5(a) (see Supplemental Material [39] for details).

In the red and blue area in Fig. 5(a), the K - and M -type structures are mainly realized, respectively. In the limited area indicated by the yellow squares near the phase boundary

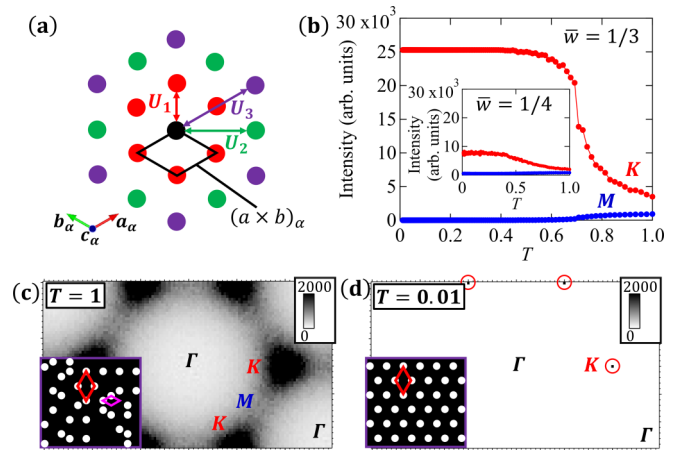


FIG. 4. (a) Schematic of the MC simulations. Circles indicate the Cu^+ ion sites. (b)–(d) Calculation results using the parameters $U_1 = 1$, $U_2 = 0$, and $U_3 = 0$. (b) Temperature dependence of the intensity in the $\bar{w} = 1/3$ system at the K (red) and M (blue) points. Inset of (b): that in the $\bar{w} = 1/4$ system. Simulated diffraction patterns in the $\bar{w} = 1/3$ system at (c) $T = 1$ and (d) $T = 0.01$. Insets of (c),(d): the atomic arrangement at each temperature. White circles correspond to Cu^+ ions. Pink and red rhombuses indicate the unit-cell size of the 1×1 and $\sqrt{3} \times \sqrt{3}$ structures, respectively.

($U_3 > 0$), the experimental results as shown in Fig. 3(d) are well reproduced; (i) $\text{Int.}(K) < \text{Int.}(M)$ in the HT phase, and (ii) $\text{Int.}(K) > \text{Int.}(M)$ just above T_c . In this phase diagram, a finite U_3 contribution is required to reproduce the

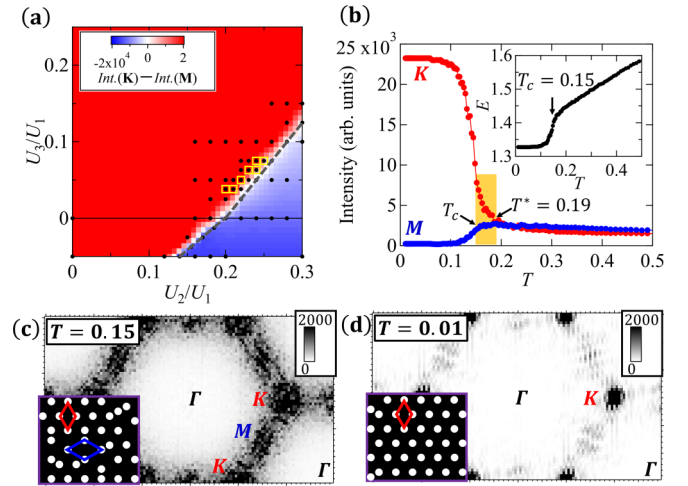


FIG. 5. (a) Color plot of the $U_3/U_1 - U_2/U_1$ ground-state phase diagram in the $\bar{w} = 1/3$ system. The intensities at $T = 0$ cooled from a random arrangement at $T = 1$ were used. The color scale indicates the difference between the intensities at the K and M points [$\text{Int.}(K) - \text{Int.}(M)$]. Black circles indicate the calculated points. (b)–(d) Calculation results using the parameters $U_1 = 1$, $U_2 = 0.22$, and $U_3 = 0.05$ in the $\bar{w} = 1/3$ system. (b) Temperature dependence of the intensity at the K (red) and M (blue) points. Inset of (b): temperature dependence of the total energy. Simulated diffraction patterns at (c) $T_c = 0.15$ and (d) $T = 0.01$. Insets of (c),(d): the atomic arrangement at each temperature. White circles correspond to Cu^+ ions. Blue and red rhombuses indicate the unit-cell size of the 2×2 and $\sqrt{3} \times \sqrt{3}$ structures, respectively.

experimental XRD data, which is reasonable considering the distance of the second- and third-nearest neighbors ($\sqrt{3}a$ and $2a$). As an example, we show the temperature dependence of the diffuse scattering with $U_1 = 1$, $U_2 = 0.22$, and $U_3 = 0.05$ [Figs. 5(b)–5(d)]. The phase transition is observable at $T_c = 0.15$ [Fig. 5(b)]. Above $T^* = 0.19$ in the HT phase, $\text{Int.}(\mathbf{K}) < \text{Int.}(\mathbf{M})$. In $T_c \leq T \leq T^*$ (yellow area), $\text{Int.}(\mathbf{K}) > \text{Int.}(\mathbf{M})$. Below T_c , the diffuse scattering at the K points condenses to form superlattice reflections, whereas the diffuse scattering at the M points disappears. Figures 5(c) and 5(d) show the diffraction patterns in plane at $T_c = 0.15$ and $T = 0.01$, respectively, which reproduce the experimental results surprisingly well [Figs. 3(b) and 3(c)] by the coordinated Cu-Cu interactions. The K - and M -type structures coexist at $T_c = 0.15$, whereas the K -type structure appears almost exclusively at $T = 0.01$ [insets of Figs. 5(c) and 5(d)]. See Fig. S10 [39] and Movie S1 for the detailed temperature dependence of the anisotropic diffuse scattering.

In the HT phase, there are two kinds of local stable environments due to the short-range Cu ordering, in which the vibrational energy of the Cu⁺ ion is different in each environment. On the other hand, only one kind of local stable environment exists in the LT phase. The existence of different environments depending on the temperature region explains that the linewidth of the E_g^{Cu} mode in the HT phase is wider than that in the LT phase [Fig. 2(g)].

If the concentration of interlayer ions decreases, the ion ordering transition temperature is expected to decrease. In fact, if only the U_1 interaction was considered ($U_2 = U_3 = 0$) in the $\bar{w} = 1/4$ system, the 2×2 ion ordered state was not realized [inset of Fig. 4(b)]. However, the experimental results show the opposite trend, in which $T_c = 280$ K in Cu_{0.24}TiSe₂ is higher than $T_c = 200$ K in Cu_{0.33}TiSe₂ [9]. On the other hand, in the $\bar{w} = 1/4$ system using the $U_1 = 1$, $U_2 = 0.22$, and $U_3 = 0.05$ interactions, which were the same values as the $\bar{w} = 1/3$ system, the complete 2×2 structure is realized below $T_c = 0.37$ (Fig. S12 [39]), whose value is higher than that of $\bar{w} = 1/3$ ($T_c = 0.15$). The results of the MC simulations are consistent with the actual system, and

suggest that there are system-dependent values for the ion concentration. The U_2 and U_3 interactions are indispensable for understanding the ion behavior in the 2D layered system, whereas these values are considered to depend on the type of ion and the host framework. Although the behavior of interlayer ions seems to involve complex correlations, this complementary approach using the observation of the diffuse scattering and the MC simulations is an effective method to understand the ion behavior owing to its filling and the interactions between ions.

IV. SUMMARY

In summary, we investigated the Cu⁺ ion behavior in the 2D layered system Cu_{0.33}TiSe₂ from multiple angles using the synchrotron XRD, IXS, first-principles calculations, and MC simulations. The large change in the E_g^{Cu} mode suggests that the Cu⁺ ions hop around triangular lattice sites in the HT phase. Our MC simulations using the coordinated Cu-Cu interactions, which are the origin of the phase transition, well reproduced the temperature dependence of the diffuse scattering. These results may be the universal behavior of intercalated ions in the 2D layered compounds. Our study provides guidelines for controlling the physical properties of intercalated layered compounds.

ACKNOWLEDGMENTS

We thank S. Kobayashi, T. Manjo, and K. Kojima for supporting the synchrotron experiments and H. Kawamura for fruitful discussions. This work was supported by a Grant-in-Aid for Scientific Research (Grants No. JP19J11697 and No. JP17K17793) from JSPS. The synchrotron radiation experiments were performed at SPring-8 with the approval of the Japan Synchrotron Radiation Research Institute (JASRI) (Proposals No. 2018A1651, No. 2018B1685 and No. 2018B1691, which are the SPring-8 Budding Researchers Support Programs, and Proposal No. 2018A1333).

-
- [1] B. L. Pauling, *J. Am. Chem. Soc.* **57**, 2680 (1935).
 - [2] D. D. Fontaine, *Solid State Phys.* **47**, 33 (1994).
 - [3] P. Mohn, *Magnetism in the Solid State* (Springer-Verlag, Berlin, 2003).
 - [4] W. Reese and L. F. May, *Phys. Rev.* **162**, 510 (1967).
 - [5] K. Takada, H. Sakurai, E. Takayama-Muromachi, F. Izumi, R. A. Dilanian, and T. Sasaki, *Nature (London)* **422**, 53 (2003).
 - [6] T. E. Weller, M. Ellerby, S. S. Saxena, R. P. Smith, and N. T. Skipper, *Nat. Phys.* **1**, 39 (2005).
 - [7] N. Katayama, M. Uchida, D. Hashizume, S. Niitaka, J. Matsuno, D. Matsumura, Y. Nishihata, J. Mizuki, N. Takeshita, A. Gauzzi, M. Nohara, and H. Takagi, *Phys. Rev. Lett.* **103**, 146405 (2009).
 - [8] M. Burrard-Lucas, D. G. Free, S. J. Sedlmaier, J. D. Wright, S. J. Cassidy, Y. Hara, A. J. Corkett, T. Lancaster, P. J. Baker, S. J. Blundell, and S. J. Clarke, *Nat. Matter.* **12**, 15 (2013).
 - [9] S. Kitou, S. Kobayashi, T. Kaneko, N. Katayama, S. Yunoki, T. Nakamura, and H. Sawa, *Phys. Rev. B* **99**, 081111(R) (2019).
 - [10] J. L. Niedziela, D. Bansal, A. F. May, J. Ding, T. Lanigan-Atkins, G. Ehlers, D. L. Abernathy, A. Said, and O. Delaire, *Nat. Phys.* **15**, 73 (2019).
 - [11] B. Li, H. Wang, K. Kawakita, Q. Zhang, M. Feygenson, H. L. Yu, D. Wu, K. Ohara, T. Kikuchi, K. Shibata, T. Yamada, X. K. Ning, Y. Chen, J. Q. He, D. Vaknin, R. Q. Wu, K. Nakajima, and M. G. Kanatzidis, *Nat. Matter.* **17**, 226 (2018).
 - [12] K. Ozawa, *Solid State Ionics* **69**, 212 (1994).
 - [13] A. Bhide and K. Hariharan, *Solid State Ionics* **192**360 (2011).
 - [14] D. Jérôme, T. M. Rice, and W. Kohn, *Phys. Rev.* **158**, 462 (1967).
 - [15] Th. Pillo, J. Hayoz, H. Berger, F. Lévy, L. Schlapbach, and P. Aebi, *Phys. Rev. B* **61**, 16213 (2000).
 - [16] T. E. Kidd, T. Miller, M. Y. Chou, and T.-C. Chiang, *Phys. Rev. Lett.* **88**, 226402 (2002).

- [17] H. Cercellier, C. Monney, F. Clerc, C. Battaglia, L. Despont, M. G. Garnier, H. Beck, P. Aebi, L. Patthey, H. Berger, and L. Forró, *Phys. Rev. Lett.* **99**, 146403 (2007).
- [18] A. Kogar, M. S. Rak, S. Vig, A. A. Husain, F. Flicker, Y. I. Joe, L. Venema, G. J. MacDougall, T. C. Chiang, E. Fradkin, J. van Wezel, and P. Abbamonte, *Science* **358**, 1314 (2017).
- [19] C. Chen, B. Singh, H. Lin, and V. M. Pereira, *Phys. Rev. Lett.* **121**, 226602 (2018).
- [20] S. Kitou, A. Nakano, S. Kobayashi, K. Sugawara, N. Katayama, N. Maejima, A. Machida, T. Watanuki, K. Ichimura, S. Tanda, T. Nakamura, and H. Sawa, *Phys. Rev. B* **99**, 104109 (2019).
- [21] E. Morosan, H. W. Zandbergen, B. S. Dennis, J. W. G. Bos, Y. Onose, T. Klimczuk, A. P. Ramirez, N. P. Ong, and R. J. Cava, *Nat. Phys.* **2**, 544 (2006).
- [22] F. J. Di Salvo, D. E. Moncton, and J. V. Waszczak, *Phys. Rev. B* **14**, 4321 (1976).
- [23] T. Atake, H. Kawaji, R. Kanno, K. Ohno, and O. Yamamoto, *Solid State Ionics* **53**, 1260 (1992).
- [24] H. Liu, X. Shi, F. Xu, L. Zhang, W. Zhang, L. Chen, Q. Li, C. Uher, T. Day, and G. J. Snyder, *Nat. Mater.* **11**, 422 (2012).
- [25] A. A. Titov, A. I. Merentsov, A. E. Kar'kin, A. N. Tiov, and V. V. Fedorenko, *Phys. Solid State* **51**, 230 (2009).
- [26] K. Sugimoto, H. Ohsumi, S. Aoyagi, E. Nishibori, C. Moriyoshi, Y. Kuroiwa, H. Sawa, and M. Takata, *AIP Conf. Proc.* **1234**, 887 (2010).
- [27] A. Q. R. Baron, Y. Tanaka, S. Goto, K. Takeshita, T. Matsushita, and T. Ishikawa, *J. Phys. Chem. Solids* **61**, 461 (2000).
- [28] X. Gonze *et al.*, *Comput. Phys. Commun.* **180**, 2582 (2009).
- [29] X. Gonze *et al.*, *Comput. Phys. Commun.* **205**, 106 (2016).
- [30] J. P. Perdew and Y. Wang, *Phys. Rev. B* **45**, 13244 (1992).
- [31] P. E. Blöchl, *Phys. Rev. B* **50**, 17953 (1994).
- [32] M. Torrent, F. Jollet, F. Bottin, G. Zérah, and X. Gonze, *Comput. Mater. Sci.* **42**, 337 (2008).
- [33] N. A. W. Holzwarth, A. R. Tackett, and G. E. Matthews, *Comput. Phys. Commun.* **135**, 329 (2001).
- [34] H. J. Monkhorst and J. D. Pack, *Phys. Rev. B* **13**, 5188 (1976).
- [35] X. Gonze, *Phys. Rev. B* **55**, 10337 (1997).
- [36] X. Gonze and C. Lee, *Phys. Rev. B* **55**, 10355 (1997).
- [37] K. Wakiya, T. Onimaru, S. Tsutsui, T. Hasegawa, K. T. Matsumoto, N. Nagasawa, A. Q. R. Baron, N. Ogita, M. Udagawa, and T. Takabatake, *Phys. Rev. B* **93**, 064105 (2016); the calculation formula of IXS is written in its Supplemental Material.
- [38] N. Metropolis, A. W. Rosenbluth, M. N. Rosenbluth, and A. H. Teller, *J. Chem. Phys.* **21**, 1087 (1953).
- [39] See Supplemental Material at <http://link.aps.org/supplemental/10.1103/PhysRevB.101.094108> for the detail of the structural parameters, the DFPT calculations, the IXS spectra, and the MC simulations.
- [40] F. Weber, S. Rosenkranz, J.-P. Castellan, R. Osborn, G. Karapetrov, R. Hott, R. Heid, K.-P. Bohnen, and A. Alatas, *Phys. Rev. Lett.* **107**, 266401 (2011).